Generalized theory of annularly bounded helicon waves

Masayuki Yano[a] and Mitchell L. R. Walker[b]
Department of Aerospace Engineering, Georgia Institute of Technology, Atlanta, Georgia 30332

(Received 9 October 2006; accepted 22 February 2007; published online 29 March 2007)

The generalized dispersion relationship for annularly bounded helicon plasma is derived. The theory considers the effect of finite electron mass, which results in the plasma field described by superposition of classical helicon solution and the Trivelpiece-Gould (TG) wave. The solution is obtained for an insulating boundary. The solution shows that the wave structure is heavily affected by the presence of the TG wave, even when a strong axial magnetic field is applied. However, the electric field profile shows that a pair of external rf antennas can still be coupled to the strong radial electric field in the plasma to excite the wave. Moreover, the general solution permits an almost continuous spectrum of parallel wave numbers. The study of k-f and n_0-B_0 diagrams shows that the linear relation obtained using classical theory holds everywhere except at low applied magnetic field strength. © *2007 American Institute of Physics*. [DOI: 10.1063/1.2716663]

I. INTRODUCTION

A helicon plasma source is a high density, high efficiency plasma source that sustains steady plasma production through the absorption and propagation of helicon waves.[1,2] The wave is launched by applying an axial magnetic field, while coupling an rf antenna to the plasma column. To date, helicon waves have only been excited in cylindrical sources. However, if the helicon plasma can be excited in a coaxial configuration, the source can be used as an ionization stage for Hall effect thrusters (HETs) and other coaxial accelerators.[3]

Currently, the efficiency of the HET is limited by the electron bombardment process, as reflected in a relatively low anode efficiency.[4] Thus, replacing the dc electron bombardment ionization stage with a high-efficiency helicon source can potentially improve the overall performance of HETs. However, a cylindrical helicon source is not suited for the ionization stage of a HET because the thruster has a coaxial acceleration stage; guiding cylindrical plasma into an annularly shaped acceleration stage is expected to cause a large loss. A solution to this problem is to develop an annular helicon plasma source that feeds directly into the rear of the HET acceleration stage. Thus, the potential increase in the efficiency and thrust-to-power ratio of the HET motivates the development of an annular helicon plasma source.

In the previous treatment of annularly bounded helicon waves,[5] several limitations are imposed in the derivation. First, the analysis neglects the finite electron mass effect. Therefore, only the helicon branch of the dispersion relationship is considered, which neglects the so-called Trivelpiece-Gould (TG) wave. As will be shown later, the TG wave has considerable effect on the field shape in helicon plasmas, even in the presence of a strong applied magnetic field. Second, the analysis assumes that the radial magnetic field vanishes at the inner and outer boundaries, and that the magnetic field outside of plasma is negligible. This boundary condition is only physically accurate for a conducting boundary condition. In reality, helicon plasma is contained in an insulator, such as Pyrex or quartz, so that it can be excited with external rf antennas. The boundary condition across an insulator requires the magnetic field to be continuous across the interface; thus, finite magnetic fields exist in the vacuum regions.

In response to the limitations of the previous analysis, this paper presents the generalized theory of annularly bounded helicon plasma, which considers the finite electron mass effect and insulating boundary conditions. Furthermore, the results of the analyses are presented so that the solution based on the classical helicon theory and the generalized theory can be compared.

II. FIELD CALCULATIONS

Figure 1 shows the physical configuration of the modeled annular helicon source. As the figure shows, the plasma is bounded by insulating material at $r=a$ and $r=b$, where r is the radius from the centerline of the device. Furthermore, it is assumed that the wave is bounded by a cylindrical conducting boundary at some radius much greater than b. Thus, the wave must vanish as $r\rightarrow\infty$. However, in actuality, the wave field in the vacuum field is highly evanescent because the wave number in the plasma region is typically a few orders of magnitude greater than that in the vacuum region. Therefore, as long as the conducting boundary is located some distance away from the plasma body, the wave field in the plasma region is insensitive to the exact location of the outer conducting boundary.[6]

The helicon dispersion relationship is derived from Maxwell's equations and the electron fluid equation of motion. A steady magnetic field, B_0, is applied in the z direction. For simplicity, the solution of the form

[a]Undergraduate Student Researcher, High-Power Electric Propulsion Laboratory, Department of Aerospace Engineering, 270 Ferst Drive, Atlanta, Georgia 30332.
[b]Assistant Professor, High-Power Electric Propulsion Laboratory, Department of Aerospace Engineering, 449 Guggenheim Building, 270 Ferst Drive, Atlanta, Georgia 30332.

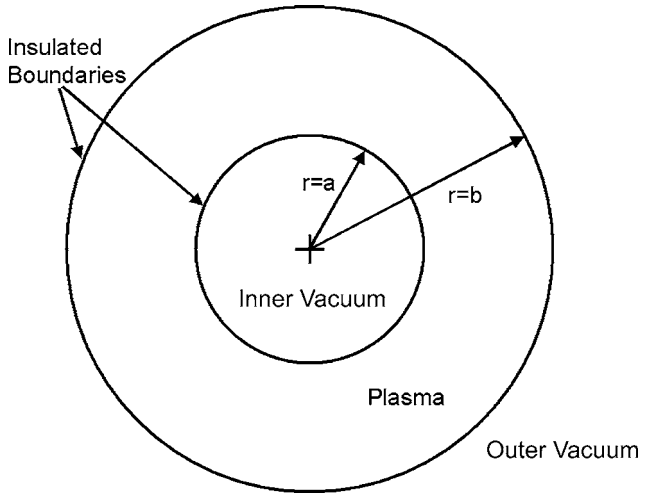

FIG. 1. Annularly bounded helicon plasma configuration.

$$\mathbf{B}(r,\theta,z,t) = (B_r(r)\hat{r} + B_\theta(r)\hat{\theta} + B_z(r)\hat{z})\exp(i(m\theta + kz - \omega t)) \tag{1}$$

is considered, where m is the mode number, k is the parallel wave number, and ω is the angular frequency of the wave. In this coordinate system, Maxwell's equations are

$$\nabla \cdot \mathbf{B} = 0 \tag{2}$$

$$\nabla \times \mathbf{E} = i\omega\mathbf{B} \tag{3}$$

$$\nabla \times \mathbf{B} = \mu_0(\mathbf{j} - i\omega\varepsilon_0\mathbf{E}), \tag{4}$$

where B, E, and j are the perturbed magnetic field, electric field, and current with respect to equilibrium. The displacement current in Eq. (4) is neglected for calculation of the plasma field, as it is always negligible in experiments.[6,7] However, the displacement current is included in the initial vacuum field calculation. The electron fluid equation of motion is

$$-\omega m_e\mathbf{v} = -e(\mathbf{E} + \mathbf{v} \times \mathbf{B}_0) - m_e\nu\mathbf{v}, \tag{5}$$

where ν is the theoretical collision rate that takes all dissipation mechanisms into account.[6] The magnetic viscosity and pressure terms are neglected from Eq. (5), as these terms play a negligible role in helicon plasmas in which the electron temperature is typically around 3 eV and the Larmor radius is much smaller than wavelength of the perturbed field.[1,6,7] In the following analysis, uniform plasma density is assumed. Moreover, the ion current is neglected because the wave frequency is much greater than lower-hybrid frequency. Thus, assuming quasineutral plasma, the plasma current is

$$\mathbf{j} = -en_0\mathbf{v}, \tag{6}$$

where n_0 is the number density. Substitution of Eq. (6) into Eq. (5) yields

$$\mathbf{E} = -\frac{B_0}{en_0}(i\delta\mathbf{j} + \hat{z} \times \mathbf{j}), \tag{7}$$

where

$$\delta = (\omega + i\nu)/\omega_c \tag{8}$$

and ω_c is the electron cyclotron frequency.[6] Neglecting displacement current, the combination of Eqs. (3), (4), and (7) yields an equation with B as the single variable. The curl of Eq. (7) is

$$\nabla \times \mathbf{E} = -\frac{B_0}{en_0}(i\delta\nabla \times \mathbf{j} + \nabla \times (\hat{z} \times \mathbf{j})). \tag{9}$$

Once again neglecting displacement current, the substitution of the curl of Eq. (4) eliminates the current terms from Eq. (9), i.e.,

$$\nabla \times \mathbf{E} = -\frac{B_0}{en_0\mu_0}(i\delta\nabla \times (\nabla \times \mathbf{B}) + \nabla \times (\hat{z} \times (\nabla \times \mathbf{B}))). \tag{10}$$

The combination of Eqs. (10) and (3) yields

$$i\omega\mathbf{B} = -\frac{B_0}{en_0\mu_0}[i\delta\nabla \times (\nabla \times \mathbf{B}) + \nabla \times (\hat{z} \times (\nabla \times \mathbf{B}))]. \tag{11}$$

Rearranging Eq. (11) results in

$$\delta\nabla \times (\nabla \times \mathbf{B}) - i\nabla \times (\hat{z} \times (\nabla \times \mathbf{B})) + \frac{\omega en_0\mu_0}{B_0}\mathbf{B} = 0. \tag{12}$$

Expansion of the second term of Eq. (12) with Eq. (1) substituted for the magnetic field yields,

$$i\nabla \times (\nabla \times \mathbf{B}) = k\left[\left(\frac{im}{r}B_z - ikB_\theta\right)\hat{r} + (ikB_r - B_z')\hat{\theta} + \frac{1}{r}(B_\theta + rB_\theta' - imB_r)\hat{z}\right]. \tag{13}$$

The expression in square brackets is identical to $\nabla \times \mathbf{B}$. Equation (12) is further simplified by defining variables

$$k_w^2 \equiv \delta k_s^2 = \frac{\omega en_0\mu_0}{B_0}, \tag{14}$$

$$k_s \equiv \omega_p/c, \tag{15}$$

$$\omega_p^2 \equiv ne^2/\varepsilon_0 m_e. \tag{16}$$

The quantity k_w is the wave number of whistler waves propagating along the magnetic field in free space,[6] ω_p is the plasma frequency, and k_s is the skin number, which is the inverse of skin depth.[8] With these substitutions, Eq. (12) simplifies to

$$\delta\nabla \times \nabla \times \mathbf{B} - k\nabla \times \mathbf{B} + k_w^2\mathbf{B} = 0. \tag{17}$$

Next we seek to derive a general solution to Eq. (17). Equation (17) is factored into[6,7]

$$(\beta_1 - \nabla \times)(\beta_2 - \nabla \times)\mathbf{B} = 0, \tag{18}$$

where β_1 and β_2 are the roots of the equation

$$\delta\beta^2 - k\beta + k_w^2 = 0. \tag{19}$$

The roots of the equation are

$$\beta_{1,2} = \frac{k}{2\delta}\left[1 \mp \left(1 - \frac{4\delta k_w^2}{k^2}\right)\right]. \tag{20}$$

Thus, the general solution to Eq. (18) is the superposition of solutions to

$$\nabla \times \mathbf{B} = \beta_j \mathbf{B}, \tag{21}$$

where $j=1,2$. Taking the curl of Eq. (21) and imposing Eq. (2) yields a set of Helmholtz equations

$$\nabla^2 \mathbf{B} + \beta_j^2 \mathbf{B} = 0. \tag{22}$$

The solution to Eq. (22) with $j=1$ corresponds to a classical helicon wave, and the solution to Eq. (22) with $j=2$ corresponds to the so-called Trivelpiece-Gould wave, or TG wave.[6,9]

The perturbed magnetic fields are obtained from Eqs. (21) and (22). The axial component of the wave is obtained from the z component of Eq. (22), which is

$$B_z'' + (1/r)B_z' + (\beta_j^2 - k^2 - m^2/r^2)B_z = 0, \tag{23}$$

where B_z'' and B_z' represent the first and second derivative of B_z with respect to r, respectively. This is a Bessel equation. Thus, in general, B_z is of the form

$$B_{zj} = C_{1j}J_m(T_j r) + C_{2j}Y_m(T_j r), \tag{24}$$

where

$$T_j^2 = \beta_j^2 - k^2, \tag{25}$$

and J_m and Y_m are the Bessel functions of the first and second kind, respectively. Unlike cylindrical cases, Y_m also provides a valid base function since the plasma region does not contain the origin. Radial and azimuthal components are obtained from r and θ components of Eq. (21), which are

$$E(im/r)B_z - ikB_\theta = \beta_j B_r \tag{26}$$

and

$$ikB_r - B_z' = \beta_j B_\theta. \tag{27}$$

Equations (26) and (27) are rearranged to express B_r and B_θ as functions of B_z and its derivative:

$$B_r = (1/T_j)\lfloor \beta_j (im/r)B_z + ikB_z' \rfloor \tag{28}$$

$$B_r = (1/T_j)\lfloor -(km/r)B_z - \beta_j B_z' \rfloor. \tag{29}$$

Equations (24), (28), and (29) are simplified by replacing C_{1j} and C_{2j} of Eq. (24) with $-2iA_jT_j$ and $-2iB_jT_j$.[1] Applying the recursive identity of the Bessel function to B_z', the perturbed magnetic fields B_r, B_θ, and B_z are expressed as

$$B_{rj} = A_j\lfloor(\beta_j + k)J_{m-1}(T_j r) + (\beta_j - k)J_{m+1}(T_j r)\rfloor + B_j\lfloor i(\beta_j + k)Y_{m-1}(T_j r) + (\beta_j - k)Y_{m+1}(T_j r)\rfloor \tag{30}$$

$$B_{\theta j} = A_j\lfloor i\{(\beta_j + k)J_{m-1}(T_j r) - (\beta_j - k)J_{m+1}(T_j r)\}\rfloor + B_j\lfloor\{(\beta_j + k)Y_{m-1}(T_j r) - (\beta_j - k)Y_{m+1}(T_j r)\}\rfloor \tag{31}$$

$$B_{zj} = A_j\lfloor -2iT_jJ_m(T_j r)\rfloor + B_j\lfloor -2iT_jY_m(T_j r)\rfloor. \tag{32}$$

Thus, in uniform annular plasma, a set of four functions constitutes the basis for the plasma field: permutation of Bessel functions of the first and second kind with arguments $T_1 r$ and $T_2 r$. As Eqs. (30)–(32) show, the basis functions in the plasma region, which are in square brackets, are uniquely determined if k, ω, n_0, and B_0 are specified.

The upper and lower bounds of the parallel number k are obtained from Eqs. (19) and (25). Differentiation of Eq. (19) with respect to β yields the minimum k given by[6]

$$k_{\min} = 2\delta k_s. \tag{33}$$

If the total wave number, T, is required to be real, then Eq. (25) requires $k \le \beta$. Then, the upper bound of k is obtained by solving Eq. (19) for $k=\beta$, i.e.,[6]

$$k_{\max} = \sqrt{\frac{\delta}{1-\delta}}k_s. \tag{34}$$

As Chen points out, the lower and upper bound of k converge for very low B_0; only the TG wave can exist in regions of low magnetic field.[6]

The radial and azimuthal components of the field described in Eqs. (30) and (31) can be represented in a more compact form if right- and left-hand circularized components are used instead.[1,6] The coordinate transfer is described by

$$\begin{bmatrix} B^R \\ B^L \end{bmatrix} = \frac{1}{\sqrt{2}}\begin{bmatrix} 1 & -i \\ 1 & i \end{bmatrix}\begin{bmatrix} B_r \\ B_\theta \end{bmatrix}. \tag{35}$$

Using this coordinate system, the magnetic fields are expressed as

$$B_j^R = A_j\lfloor\sqrt{2}(\beta_j + k)J_{m-1}(T_j r)\rfloor + B_j\lfloor\sqrt{2}(\beta_j + k)Y_{m-1}(T_j r)\rfloor \tag{36}$$

$$B_j^L = A_j\lfloor\sqrt{2}(\beta_j - k)J_{m+1}(T_j r)\rfloor + B_j\lfloor\sqrt{2}(\beta_j - k)Y_{m+1}(T_j r)\rfloor. \tag{37}$$

The calculation of the vacuum field is conducted in a similar manner. However, in a vacuum, the conduction current is zero, but the displacement current may not be negligible. Thus, Eqs. (3) and (4) yield

$$\nabla \times (\nabla \times \mathbf{B}) = k_0^2 \mathbf{B}, \tag{38}$$

where $k_0 \equiv \omega/c$. Then, imposing Eq. (2) on Eq. (38) results in

$$\nabla^2 \mathbf{B} + k_0^2 \mathbf{B} = 0. \tag{39}$$

For helicon waves, $k \gg k_0$, the solution is described using the modified Bessel functions. The basis function for the inner vacuum region is $I_m(T_3 r)$, which is finite at the origin, and the basis function for the outer vacuum is $K_m(T_4 r)$, which goes to zero as r tends to infinity. In the circularly polarized coordinate system, the solution to the inner vacuum region is

$$B_3^R = C_1\lfloor\sqrt{2}I_{m-1}(T_3 r)\rfloor \tag{40}$$

$$B_3^L = C_2\lfloor\sqrt{2}I_{m+1}(T_3 r)\rfloor \tag{41}$$

$$B_{3z} = C_1[-i(T_3/k)I_{m+1}(T_3r)] + C_2[-i(T_3/k)I_{m+1}(T_3r)], \tag{42}$$

where

$$T_3^2 = -(k_0^2 - k^2). \tag{43}$$

Similarly, the solution to the outer vacuum region is

$$B_4^R = D_1[\sqrt{2}K_{m-1}(T_3r)] \tag{44}$$

$$B_4^L = D_2[\sqrt{2}K_{m+1}(T_3r)] \tag{45}$$

$$B_{3z} = D_1[-i(T_3/k)K_{m+1}(T_3r)] + D_2[-i(T_3/k)K_{m+1}(T_3r)]. \tag{46}$$

Thus, when the displacement current is included in the vacuum field calculation, a set of four functions constitutes a basis for the inner and the outer vacuum field. Together with the four functions that span the plasma solution space, a basis for the total wave field consists of eight functions.

The coefficients are readily obtained by applying boundary conditions at the interface of the inner vacuum and plasma and at the interface of the outer vacuum and plasma. One of the conditions is that the radial magnetic field is continuous across the boundary.[7] Then, since the plasma can only carry finite surface current, the azimuthal and axial components of the magnetic field must also be continuous across the boundary from Eq. (4).[6,7] Finally, the tangential electric field across the boundary must be continuous.[6,9,10] This requirement is satisfied by either imposing the continuity condition on the axial or azimuthal electric fields; for simplicity, the axial field is matched in this analysis. The axial field in the plasma is obtained from[6]

$$E_z^{\text{plasma}} = -\frac{2c^2}{\omega}\frac{k_0^2}{k_s^2}\left[\sum_{j=1,2}[A_j\beta_j T_j J_m(T_j r) + A_j\beta_j T_j Y_m(T_j r)]\right]. \tag{47}$$

Evaluating the above equation at $r=a$ and $r=b$ yields the electric field at the inner and outer boundaries. On the other hand, the electric field in the vacuum can be expressed as[6]

$$E_z^{\text{in}} = \frac{c^2}{\omega}T_3(C_1 - C_2)I_m(T_3r) \tag{48}$$

and

$$E_z^{\text{out}} = \frac{c^2}{\omega}T_3(C_1 - C_2)K_m(T_3r), \tag{49}$$

where E_z^{in} and E_z^{out} are the electric fields in the inner vacuum region and outer vacuum region, respectively.

Thus, there are a total of eight boundary conditions, four at each boundary. As one of the eight unknown coefficients is a proportionality factor, there are seven free coefficients. The last degree of freedom is provided by the parallel wave number, k, which acts as an eigenvalue of the problem. The boundary conditions are expressed as an eight-by-eight linear system, and nontrivial solutions are obtained by choosing an appropriate value of k so that the matrix is singular. Although the procedure is mathematically sound, it is numerically difficult to solve. The numerical difficulty arises because the coefficients C_1-C_2 and D_1-D_2 essentially become zero. In other words, displacement current is negligible, even in the vacuum region.[6,7] If displacement current is neglected, then Eq. (39) reduces to Laplace's equation. Consequently, the inner vacuum solution simplifies to

$$B_{r3} = C[(k/2)(I_{m-1}(kr) + I_{m+1}(kr))] \tag{50}$$

$$B_{\theta 3} = C[i(m/r)I_m(kr)] \tag{51}$$

$$B_{z3} = C[ikI_m(kr)] \tag{52}$$

and the outer vacuum solution becomes

$$B_{r4} = D[-(k/2)(K_{m-1}(kr) + K_{m+1}(kr))] \tag{53}$$

$$B_{\theta 4} = D[i(m/r)K_m(kr)] \tag{54}$$

$$B_{z4} = D[ikK_m(kr)]. \tag{55}$$

The simplified solution, which neglects displacement current in the vacuum region, is used for the rest of the analysis.

The electric field in the plasma is computed from Eqs. (3) and (7). Neglecting displacement current in the plasma, the electric field can be expressed as function of magnetic field,[6] i.e.,

$$E_r = \frac{\omega}{k}B_\theta - \frac{i}{k}E_z' \tag{56}$$

and

$$E_\theta = \frac{m}{kr}E_z - \frac{\omega}{k}B_r, \tag{57}$$

where E_z and E_z' are obtained from Eq. (47).

III. WAVE FIELD ANALYSIS

The magnetic field profiles in the plasma are readily obtained from Eqs. (30)–(32) and (50)–(55). Typical magnetic field shapes in the plasma and vacuum regions are shown in Figs. 2(a)–2(c). Figure 2(a) shows the radial magnetic field profile. As the figure shows, the helicon solution dominates the TG wave. The field shape is similar to the profile obtained previously based on the classical helicon solution.[5] However, unlike the conducting boundary case studied previously, a finite radial magnetic field exists at both insulating boundaries. The wave magnitude in the inner vacuum region is an order of magnitude smaller than that in the plasma region. The outer vacuum field also attenuates rapidly with radius; in fact, the vacuum field strength at $r=2b$ is an order of magnitude smaller than that of the peak plasma field.

Figures 2(b) and 2(c) show the azimuthal and axial magnetic field shapes, respectively. Unlike the radial magnetic field, the helicon wave and the TG wave contribute equally to the total wave structure. However, as discussed in previous publications,[6,9] the TG mode is expected to be highly damped and only affects the field near the boundaries. The helicon part of the solution is similar to that obtained using the classical helicon theory. In other words, the coupling be-

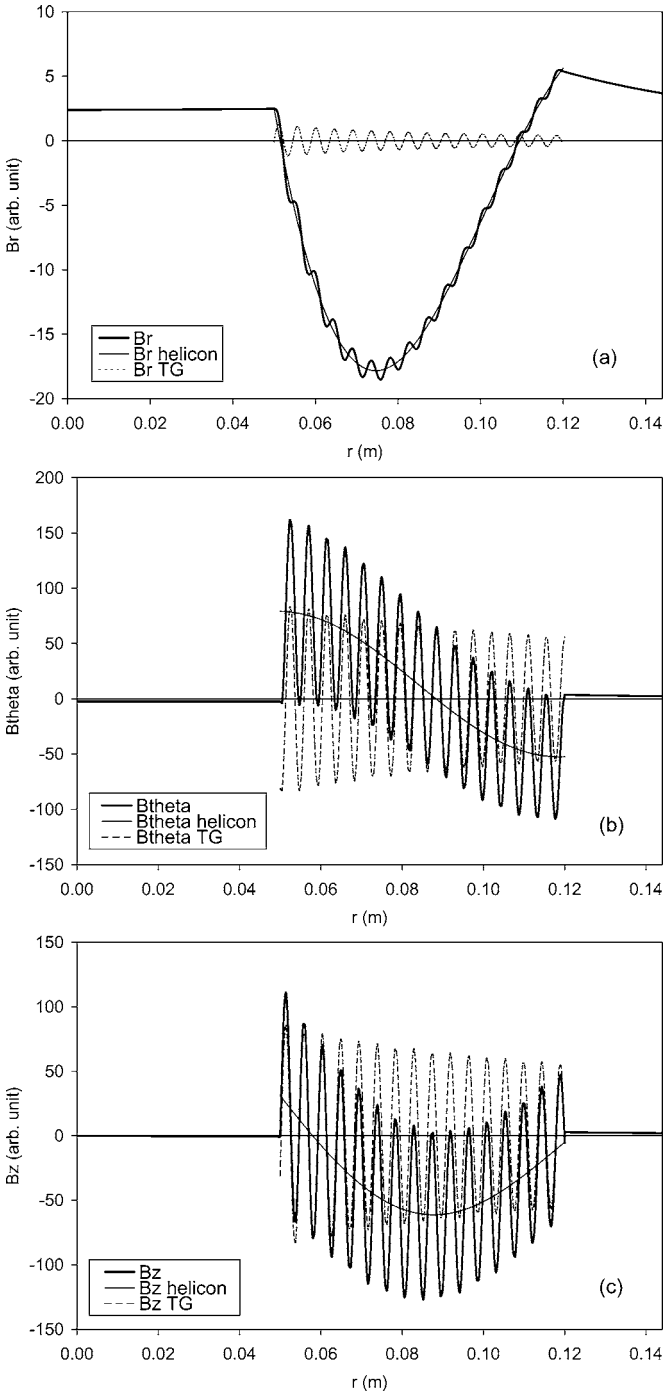

FIG. 2. Typical radial (a), azimuthal (b), and axial (c) magnetic field profiles. The thick line corresponds to the total field, the thin line represents to the helicon wave, and dotted line represents the TG wave. The configuration is $m=1$, $a=5$ cm, $b=12$ cm, $n_0=2\times10^{18}$ m^{-3}, $B_0=500$ G, $f=6$ MHz, $k=6.21$ m^{-1}.

tween the helicon mode and the TG mode is negligible when the wave frequency is much less than the electron cyclotron frequency; a significant coupling occurs only when the applied magnetic field is weak and the wave number of helicon and TG modes are comparable.[6] The helicon and TG wave nearly cancel each other at both boundaries. Therefore, the magnetic fields in the vacuum regions are much weaker than that in the plasma. Again, the magnetic field in the outer vacuum region is highly evanescent.

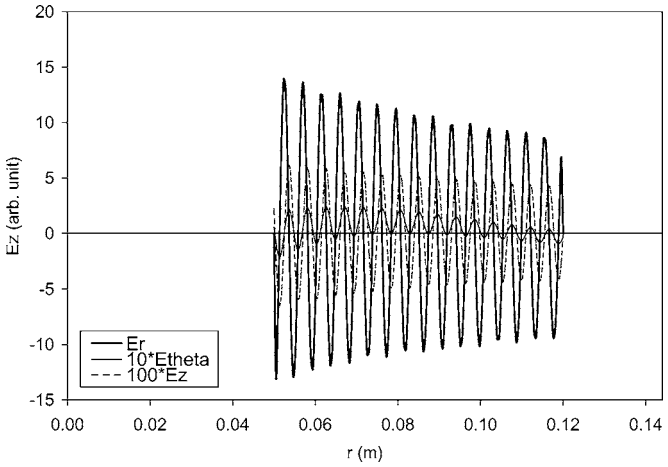

FIG. 3. Typical electric field profile. The magnitudes of the waves are scaled by the coefficients given in the legend.

Figure 3 shows the electric field shape, computed from Eqs. (47), (56), and (57). In this figure, the magnitude of each profile is adjusted by the factors defined in the legend. The electric field in the radial direction is much stronger than the electric field in the azimuthal or axial direction. Thus, the radial component of the electric field dominates the overall electric field structure. Although the field appears to fluctuate rapidly with radius due to the presence of the TG mode, the TG wave in the body of the plasma would be highly evanescence when damping is considered.[9] Thus, the electric field structure far from the boundaries is expected to be similar to that obtained using classical helicon theory.[5] Therefore, the field can be excited with an external source by inducing an outward electric field at $\theta=0°$ and an inward electric field at $\theta=180°$. This applied electric field topography can be realized by using two sets of rf antennas, one inside and the other outside the plasma. Antenna coupling can be improved by employing helical antennas with a twist rate equal to the rotation rate of the helicon wave; this configuration allows the antennas to exactly match the electric field spatially twice while the helicon wave completes one rotation.[11]

The eigenvalue condition for satisfying the boundary conditions is also studied. Physically, the eigenvalue of the problem is equal to the parallel wave number, k. Figure 4 shows the variation of the matrix determinant used for boundary condition matching. The wave can exist in the plasma when the matrix is singular, which occurs at each zero crossing. Unlike the solution based on the classical helicon wave alone,[1,5] multiple eigenvalues exist when the TG wave is included. Furthermore, although the values of k are discrete, zero crossing occurs very frequently. Therefore, the wave can exist in a nearly continuous spectrum of values of k varying from $k_{\min}$ to $k_{\max}$. A similar result has been obtained for a cylindrical source previously.[6] However, the fine discretization of the field occurs only when the applied magnetic field strength is strong, such that the ratio of ω/ω_c is small. If the ratio of ω/ω_c is large, coupling of the helicon and TG modes occurs and the number of zero crossings decreases. In fact, as the ratio of ω/ω_c approaches 1/2, the total wave number of the helicon branch and the TG branch de-

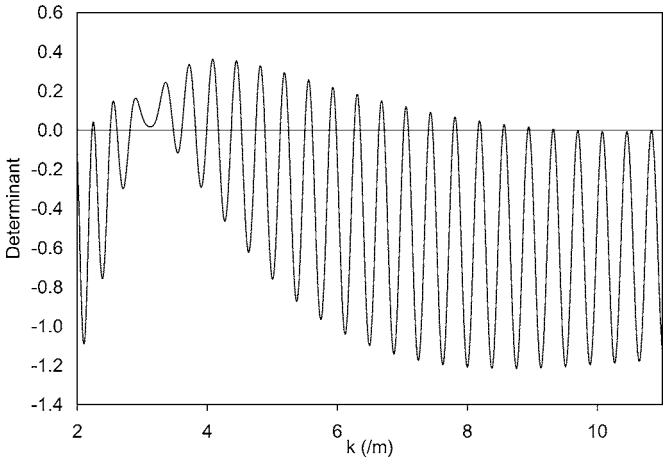

FIG. 4. The eigenvalue condition for boundary condition matching. The y value corresponds to the determinant of the matrix used to match the boundary values. The solution is realized at each zero crossing.

scribed in Eq. (20) converges;[6] in such a weak magnetic field, the helicon wave cannot propagate and the wave becomes a TGould wave.

Figure 5 shows the ratio of the TG wave-to-helicon wave maximum amplitude as a function of k for the radial, azimuthal, and axial magnetic field. As the graph shows, the ratio of the TG-to-helicon wave amplitude is less than unity for the radial magnetic for the entire spectrum of k. The ratio generally decreases with an increase in the parallel wave number. On the other hand, the ratio of the TG-to-helicon wave amplitude is greater than unity for B_θ and B_z. Furthermore, the ratio of azimuthal components fluctuates between unity and a number greater than unity. The ratio of axial components also fluctuates above $k=6$ m^{-1}. Thus, the wave structure changes at each zero crossing. Unlike the radial component, the ratio of the helicon to TG wave amplitude generally increases with the parallel wave number for azimuthal and axial components. Note, that the wave profiles shown in Figs. 2(a)–2(c) are those obtained at the lower end

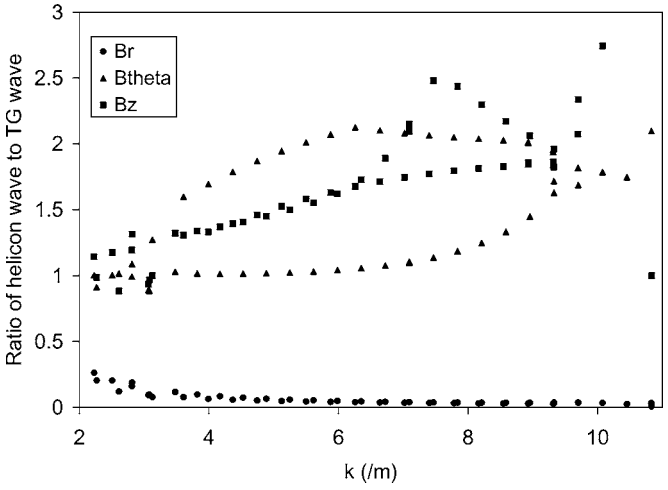

FIG. 5. The ratio of magnitudes of classical helicon solution and the TG solution as a function of wave number.

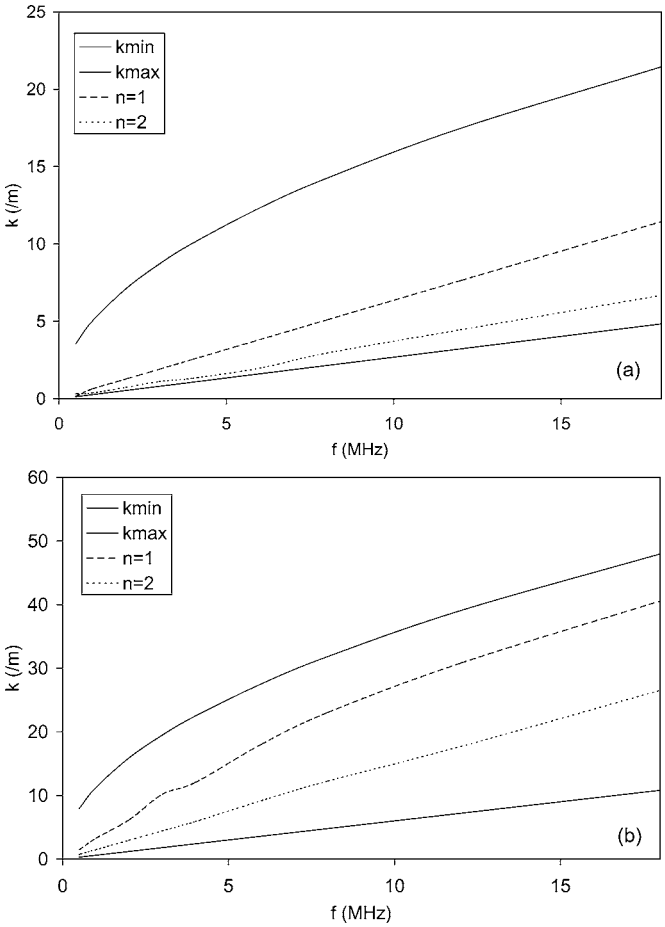

FIG. 6. A diagram showing a typical variation of the wave number as a function of frequency. The k_{max} and k_{min} corresponds to the upper and lower bounds of the wave number, respectively. Wave number for approximate $n=1$ mode and $n=2$ mode are also shown. $n_0=10^{18}$ m^{-3} (a) and $n_0=5\times10^{18}$ m^{-3} (b).

of the k spectrum; therefore, the ratio of the TG-to-helicon wave amplitudes in the azimuthal and axial direction are close to unity.

IV. k-f AND n_0-B_0 ANALYSES

The relationship between the parallel wave number, k, and frequency is analyzed for different sets of wave structures. Figures 6(a) and 6(b) show the results of the computation for electron number densities, n_0, of 10^{18} and 5×10^{18} m^{-3}, respectively. All geometric parameters used in the analysis are the same as those used in analysis of the wave field profiles. The mode shapes used to classify the wave structure are defined as follows:

1. $n=1$: the B_r component of helicon branch becomes nearly zero at both the inner and outer boundary without crossing zero in between;
2. $n=2$: the B_r component of helicon branch becomes nearly zero with one zero crossing near the midpoint.

This is analogous to the method used to describe the different modes of the classical helicon wave.[12] For example, the wave structure shown in Fig. 1(a) is closest to the $n=1$ mode.

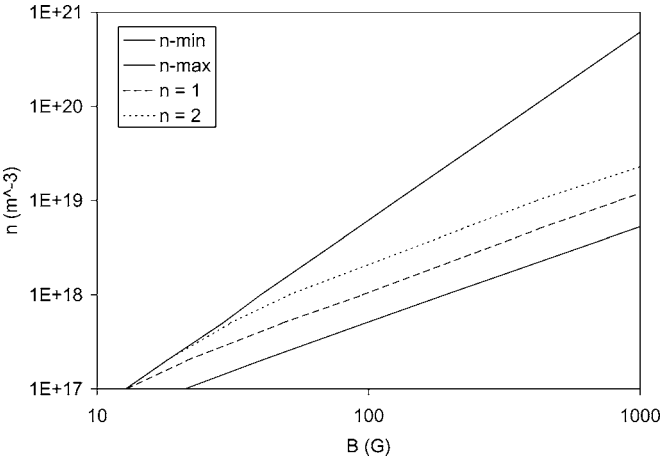

FIG. 7. A diagram showing a typical variation of the number density as a function of magnetic field strength. The maximum density (n-max) and the minimum density (n-min), and the density of approximate $n=1$ and $n=2$ modes are shown. Configuration: $k=20$ m^{-1}; $f=6$ MHz.

Figures 6(a) and 6(b) show that the parallel wave number increases with frequency in general. The $n=1$ mode has a higher wave number than the $n=2$ mode for a given frequency. Thus, the number of zero crossings in the radial wave profile increases with the decrease in the wave number in general, i.e., the radial magnetic field fluctuates more rapidly with respect to space for lower k. Furthermore, k varies linearly with f for frequencies above 6 MHz; this implies that the wave velocity, $v_w=\omega/k$, is essentially constant for a given wave structure and applied field strength. In addition, the steeper f/k slope of the $n=2$ mode implies that the wave propagates faster in this mode. The difference in the speed of propagation can effect the rate of energy deposition.[1,12] The comparison of Figs. 6(a) and 6(b) shows that the wave number increases as the plasma density increases. Moreover, k corresponding to the $n=1$ mode increases relative to $k_{\min}$ and $k_{\max}$ at higher density. In reality, the value of k is determined by the energy absorption mechanism for a given f and B_0.[9] It has been experimentally observed that the wave structure changes from $n=1$ mode to $n=2$ mode at high power.[12]

For practical purposes, it is useful to know the variation of the plasma number density as a function of applied magnetic field strength. In previous studies using the classical helicon solution, it was found that the density of plasma varies linearly with the applied magnetic field strength for a given frequency.[1,5] Figure 7 shows a typical diagram of the number density as a function of applied magnetic field strength using the generalized theory. The figure shows the maximum and minimum number density attainable at a given magnetic field strength, $n_{0\,\max}$ and $n_{0\,\min}$, respectively. The figure also shows the densities for the $n=1$ and $n=2$ modes. The minimum and maximum number density can be conceived as the range of plasma density for which wave can propagate at a given applied field strength. For both the $n=1$ and $n=2$ modes, the number density increases linearly with the applied magnetic field strength for field strengths greater than 80 G, which agrees with the results from classical theory. However, in the low magnetic field region, the density varies nonlinearly with the applied field strength. In fact, the diagram reveals some minimum threshold magnetic field strength below which the wave cannot propagate. Furthermore, the minimum threshold for the $n=2$ mode is higher than that for the $n=1$ structure. In this low field region, the ratio of β_2-to-β_1 approaches unity, which causes the helicon wave and TG wave to behave similarly. In general, the $n=2$ mode has a higher number density than the $n=1$ mode, which agrees with experimental observations.[12]

V. CONCLUSION

The electric and magnetic field solution of an annularly bounded helicon wave is obtained using the generalized theory, which considers both the classical helicon wave and Trivelpiece-Gould wave. The boundary conditions are also corrected for an insulating boundary; with the modification, the wave field in the vacuum regions is also considered. Although the radial magnetic field profile is similar to that based on classical helicon solution, the azimuthal and axial field profiles are strongly affected by the presence of the TG wave. However, the TG wave is expected to be highly evanescent in the body of plasma when damping is considered. The strong radial electric field is still present, and a pair of externally located rf antennas can excite the wave. Moreover, the eigenvalue analysis shows that the generalized theory permits an almost continuous spectrum of parallel wave numbers, varying from $k_{\min}$ to $k_{\max}$. It is also shown that the wave velocity is essentially constant for a given wave structure above a certain frequency. Furthermore, the number density varies linearly with the applied magnetic field strength as predicted by classical helicon theory, except in the very low field configuration.

[1] F. F. Chen, Plasma Phys. Controlled Fusion **33**, 339 (1991).
[2] R. W. Boswell, Plasma Phys. Controlled Fusion **26**, 1147 (1984).
[3] V. V. Zhurin, H. R. Kaufman, and R. S. Robinson, Plasma Sources Sci. Technol. **8**, R1 (1999).
[4] R. R. Hofer and A. D. Gallimore, J. Propul. Power **22**, 732 (2006).
[5] M. Yano and M. Walker, Phys. Plasmas **13**, 063501 (2006).
[6] F. F. Chen and D. Arnush, Phys. Plasmas **4**, 3411 (1997).
[7] J. P. Klozenberg, B. McNamara, and P. C. Thonemann, J. Fluid Mech. **21**, 545 (1965).
[8] F. F. Chen, *Introduction to Plasma Physics and Controlled Fusion* (Plenum, New York, 1984), Vol. 1.
[9] D. Arnush and F. F. Chen, Phys. Plasmas **5**, 1239 (1998).
[10] D. Arnush, Phys. Plasmas **7**, 3042 (2000).
[11] D. G. Miljak and F. F. Chen, Plasma Sources Sci. Technol. **7**, 61 (1998).
[12] J. P. Rayner and A. D. Cheetham, Plasma Sources Sci. Technol. **8**, 79 (1999).